inorganics

MDPI

Article

Molten Salt Synthesis of Micro-Sized Hexagonally Shaped $REMnO_3$ (RE = Y, Er, Tm, Yb)

Dovydas Karoblis, Aleksej Zarkov *, Tomas Murauskas and Aivaras Kareiva

Institute of Chemistry, Vilnius University, Naugarduko 24, LT-03225 Vilnius, Lithuania
* Correspondence: aleksej.zarkov@chf.vu.lt

Abstract: Yttrium manganite ($YMnO_3$) is a compound belonging to the hexagonal rare earth manganites family, which demonstrates multiferroic properties. This material can be prepared by several synthetic approaches, with the most common one being the solid-state synthesis. In this work, we show a possibility of preparing this material via molten salt synthesis using the NaCl-KCl mixture as the reaction medium and yttrium and manganese nitrates as the starting materials. We demonstrate that, by varying the reaction temperature and the nitrates-to-chlorides ratio, it is feasible to synthesize hexagonally shaped particles of microscopic dimensions. A similar synthesis procedure can be successfully applied for the preparation of other hexagonal manganites—$ErMnO_3$, $TmMnO_3$, and $YbMnO_3$.

Keywords: multiferroics; hexagonal manganites; yttrium manganite; molten salt synthesis

check for updates

Citation: Karoblis, D.; Zarkov, A.; Murauskas, T.; Kareiva, A. Molten Salt Synthesis of Micro-Sized Hexagonally Shaped $REMnO_3$ (RE = Y, Er, Tm, Yb). *Inorganics* **2023**, *11*, 178. https://doi.org/10.3390/inorganics11050178

Academic Editor: Cristina Leonelli

Received: 24 February 2023
Revised: 10 April 2023
Accepted: 18 April 2023
Published: 23 April 2023

1. Introduction

Hexagonal rare earth manganites $REMnO_3$ (RE = rare earth element) have attracted a lot of scientific attention due to the possibility of obtaining two ferroic orders in the same phase [1]. The trimer structural distortion observed in these materials leads to the appearance of polarization, as well as bulk magnetization and the linear magnetoelectric effect [2]. Rare earth manganites with hexagonal structure have antiferromagnetic ordering at lower temperatures (T_N varies in 57–130 K range) [3] and are ferroelectrics at high temperatures (T_C–620–1000 K) [4]. This type of multiferroics could be applied in energy-efficient devices [5], relying upon electric-field control of magnetism, biomedicine [6], photocatalysis [7], solid oxide fuel cells [8], gas sensors [9], etc.

Out of all the rare earth manganites with hexagonal crystal structures, $YMnO_3$ is one of the most studied. This material has a low Néel temperature (T_N~80 K) and a high Curie temperature (T_C~910 K) [10] Moreover, it displays mutual coupling between structural translation and the antiferromagnetic and ferroelectric domains walls [11]. This multiferroic vortex have been extensively investigated due to its fascinating physics and possible application in data storage devices [12]. The ferroelectric hexagonal $YMnO_3$ has a $P6_3$ cm space group and the structure of this compound consists of non-connected MnO_5 trigonal bipyramid layers with Y^{3+} layers in between [13]. In addition to demonstrating multiferroic properties, this manganite has shown photocatalytic activity towards methyl red degradation [14], a high near-infrared reflectance [15], various gas sensing abilities [16], and excellent photodetection performance [17].

Various synthetic approaches can be used for the synthesis of $YMnO_3$ in the form of nanoparticles, bulk material, or thin films [18–21]. While it has some drawbacks, solid-state synthesis is the most used method. This synthetic route usually involves several annealing stages, a long mixing of the starting materials and sintering times (more than 10 h), and high temperatures (higher than 1100 °C) [22,23]. On the other hand, different salts can be used as the reaction medium to increase the rate of diffusion for solid-state reactions. The preparation technique where metal oxides are synthesized in inorganic melt, with

temperatures slightly beyond the melting point, is known as molten salt synthesis [24]. This approach is cheap, easy to upscale, clean, does not require sophisticated equipment, and offers the possibility of obtaining uniformly shaped particles at lower temperatures and shorter reaction times [25].

Few different studies dealing with the preparation of $YMnO_3$ by molten salt synthesis have been already reported [26–28]. In all cases, either NaCl or the eutectic mixture of NaCl and KCl were used as the reaction medium. When sodium oleate was added to the reaction mixture, the formation of nanoplates transpired [28], while the use of sodium and potassium chlorides resulted in short, prism-like particles [26]. Furthermore, it was demonstrated that the reaction temperature plays a significant role in the formation of $YMnO_3$ with an orthorhombic or hexagonal structure [27]. While some work was already conducted by preparing $YMnO_3$ via molten salt synthesis, there are many different parameters, including starting materials, the use of new salts as the reaction medium, temperature, the ratio between salts and precursors, reaction time, etc., which could influence the physical properties or shape of the finals products. Moreover, there are three distinctive phases where the Y and Mn molar ratio is 1:1, such as $Y_2Mn_2O_7$ pyrochlore and orthorhombic $YMnO_3$ (which are metastable ones), as well as thermodynamically stable hexagonal $YMnO_3$ potential changes in reaction conditions could lead to the selective phase synthesis.

In our work, we present a novel way to conduct molten salt synthesis, where metal nitrates are used as the starting materials instead of oxides. We demonstrate that the temperature and precursors-to-chlorides ratio influence the formation of phase-pure hexagonal $YMnO_3$ consisting of hexagonally shaped particles without any sodium or potassium doping. We also show that this synthetic approach can be applied to prepare different hexagonal rare earth manganites, in particular $ErMnO_3$, $TmMnO_3$, and $YbMnO_3$. To the best of our knowledge, thulium and ytterbium manganites were synthesized by the molten salt method for the first time.

2. Results and Discussion

Typically, in the molten salt synthesis, metal oxides are used as the starting materials, while for the reaction medium different salts can be exploited. Since in previously reported works [26,27] yttrium and manganese (IV) oxides were used for the preparation of $YMnO_3$ by the molten salt method, we applied similar experimental conditions for comparison. The XRD patterns of the synthesis products are represented in Figure S1. As can be seen, depending on the synthesis temperature, two different phases of $YMnO_3$ can form. When annealing was performed at a lower temperature (700 °C), the main phase was $YMnO_3$ with an orthorhombic structure (o-$YMnO_3$), while a higher temperature resulted in the formation of hexagonal $YMnO_3$ (h-$YMnO_3$). In both cases, the diffraction peaks associated with the starting Y_2O_3 can be seen in the XRD profiles. Interestingly, the amount of this impurity did not change with the increase in the reaction temperature. According to Rietveld refinement, the ratio between o-$YMnO_3$ and Y_2O_3 was 94% to 6%, while the ratio between h-$YMnO_3$ and Y_2O_3 was calculated as 93% to 7%.

Since the synthesis from metal oxides did not lead to the formation of single-phase $YMnO_3$, we prepared $YMnO_3$ from the yttrium and manganese nitrates, with an expectation of the in situ formation of more reactive oxides. Firstly, we analyzed the thermal decomposition of the starting mixture consisting of nitrates and chlorides by thermogravimetric analysis; the results are demonstrated in Figure 1.

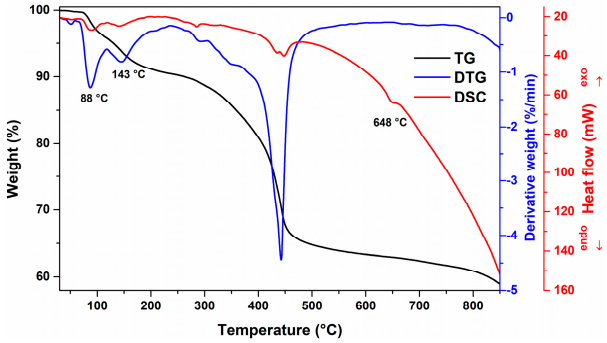

Figure 1. TG/DTG/DSC curves of starting reaction mixture of metal nitrates and alkali metal chlorides.

The DTG curve clearly reveals that the degradation of starting materials occurs in several steps. The first peak can be seen at 49 °C and could be related to the melting of manganese nitrate, where a small endotherm in the DSC curve confirms this process. Moreover, a significant weight loss can be distinguished in the 70–260 °C range with two peaks in the DTG curve, which are centered around 88 °C and 143 °C. The removal of adsorbed as well as structural water and the decomposition of manganese nitrate are the processes which may take place during this stage. According to Jian et al. [29], the degradation of manganese nitrate to manganese oxide transpires at 250 °C, which matches well with our study. The most significant weight loss (around 24% of initial mass is lost) occurs in the 300–450 °C region and could be associated with the degradation of yttrium nitrate to yttrium oxide and nitrogen oxide. In addition, a small endotherm at 648 °C in the DSC curve could be related to the melting of the eutectic NaCl-KCl mixture. Prior to the eutectic point, this salt mixture is known to be stable [30]. It is noteworthy that NaCl could potentially react with the formed MnO_2, but only in acidic conditions, which is not the case in our system. The mass is constantly decreasing from 500 °C to 850 °C and this could be explained by two processes. First of all, the complete degradation of yttrium nitrate happens at around 640 °C [31], while the latter mass decrease could be explained by the generation of oxygen gas during the reaction between the in situ formed yttrium and manganese oxides.

While it is known that the formation of o-$YMnO_3$ can transpire at lower temperatures, higher temperatures are usually used for the preparation of h-$YMnO_3$. In our case, we performed synthesis at 900 °C and 1100 °C, with the molar ratio between starting materials and chlorides being 1:2; the XRD patterns of the obtained products are given in Figure 2.

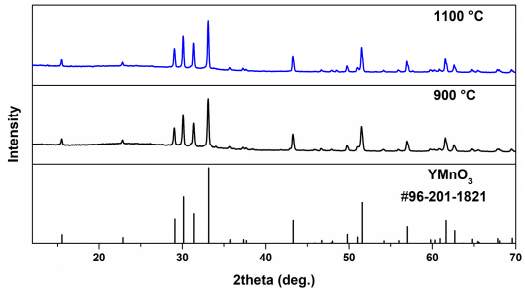

Figure 2. XRD patterns of $YMnO_3$, prepared at 900 °C and 1100 °C with the molar ratio between nitrates and chlorides as 1:2 with reaction time of 10 h.

It is clearly seen that, regardless of the temperature, h-$YMnO_3$ formed as the main crystal phase. It is worth noting that Y_2O_3 was not detected in the synthesis products. Rietveld refinement was performed for both samples and the results are presented in Table 1. The cell parameters match well with those of the h-$YMnO_3$ synthesized by the conventional solid-state method [32]. One of the advantages of the molten salt method is shorter reaction times in comparison with a solid-state reaction. For this reason, we tried to

synthesize materials, varying the reaction time at 900 °C; the results are shown in Figure S2. Shorter or prolonged reaction times did not lead to the formation of monophasic h-$YMnO_3$. When the reaction time was 1 h, few different impurity phases could be witnessed, like o-$YMnO_3$, Y_2O_3 and MnO_2, while for longer reaction times, small amounts of yttrium and manganese oxides as the neighboring phases were present.

Table 1. Cell parameters of $YMnO_3$ samples with hexagonal structure.

Synthesis Conditions		a, Å	b, Å	c, Å	V, Å^3
Temperature, °C	Molar Ratio between Precursors and Chlorides				
900	1:2	6.1490 (6)	6.1490 (6)	11.4065 (7)	373.51 (0)
1100	1:2	6.1359 (4)	6.1359 (4)	11.3902 (5)	371.38 (6)
1000	1:10	6.1432 (5)	6.1432 (5)	11.4039 (0)	372.71 (8)
1100	1:10	6.1376 (1)	6.1376 (1)	11.3907 (3)	371.60 (4)

FT-IR spectroscopy was applied in order to investigate the structure of one of the specimens, specifically the one prepared at 1100 °C; the results are presented in Figure 3.

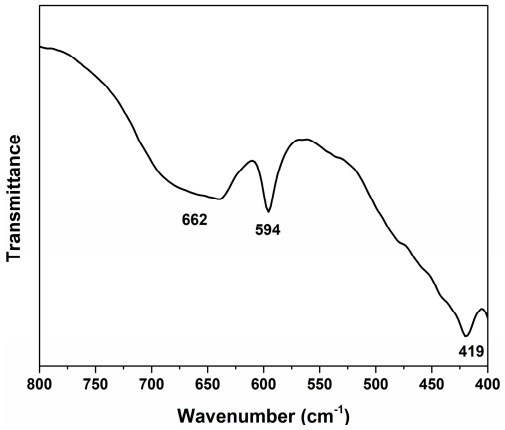

Figure 3. FT-IR spectrum of $YMnO_3$ sample synthesized at 1100 °C.

The FT-IR can be applied to distinguish the differences between an orthorhombic and a hexagonal structure [33] for similar compounds. Compounds with an orthorhombic structure have two distinguishable peaks centered at 530 and 490 cm^{-1} associated with O-Mn-O bending and Re-O vibrations, respectively, while these absorption bands are missing in the samples with hexagonal structures. For our sample, three absorption bands can be observed. The first and broad one, which is centered around 662 cm^{-1}, can be associated with the stretching Mn-O bond vibration. The sharp and more intense peak at 594 cm^{-1} corresponds to the Mn-O bond vibration in MnO_5 [34]. Lastly, the sharp peak at 419 cm^{-1} was previously observed for the Y-O bond vibration [35]. It should be noted that our sample did not contain any peaks which could be attributed to the MnO_2 phase [36], as well as peaks in the 4000–800 cm^{-1} range which usually correspond to organic groups, such as carbonates, etc.

The morphology of the specimens synthesized at 900 °C and 1100 °C with reaction times of 10 h was further investigated; the SEM images are displayed in Figure 4.

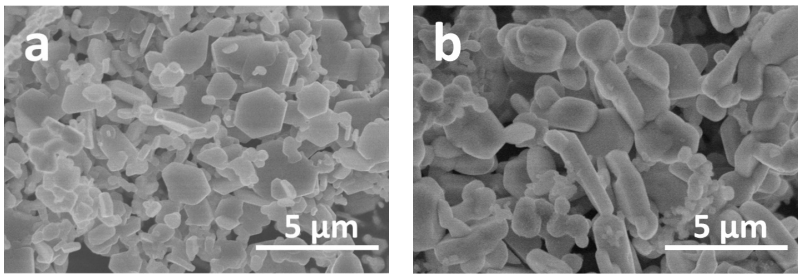

Figure 4. SEM micrographs of $YMnO_3$, prepared at 900 (**a**) and 1100 (**b**), with the ratio between nitrates and chlorides of 1:2.

The synthesis temperature influenced not only the particle size, but also the shape. For the sample prepared at 900 °C (Figure 4a), several particles with regular hexagonal and convex hexagonal shapes could be observed. The side length of these hexagons varies in the 0.5–1.5 µm range. This sample also contained smaller particles varying in nanoscale and microscale dimensions. The sample obtained at 1100 °C (Figure 4b) showed agglomerated micro-sized particles without distinctive shapes. According to the previous studies [32,37,38], h-$YMnO_3$ prepared by conventional solid-state synthesis route at similar temperatures consisted of larger agglomerates and clusters without particular shapes.

Taking into account that our proposed molten salt synthetic approach can lead to the formation of particles with well-defined hexagonal shapes, we tried to dilute the starting nitrates mixture by increasing the amount of NaCl-KCl by five times. The XRD patterns of specimens prepared at 900 °C, 1000 °C, and 1100 °C are represented in Figure 5.

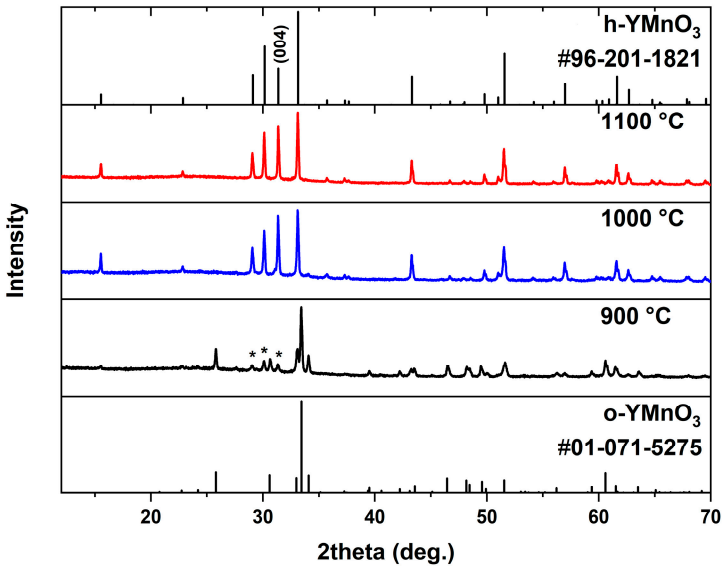

Figure 5. XRD patterns of $YMnO_3$ prepared at different temperatures with the molar ratio between precursors and chlorides 1:10. * represents the peaks belonging to the h-$YMnO_3$.

The dilution of the starting nitrates mixture with chlorides resulted in the emergence of different $YMnO_3$ structures depending on the reaction temperature. When the ratio between the starting nitrates and chlorides was 1:2, at 900 °C only hexagonal $YMnO_3$ was present, whereas with the ratio of 1:10 the mixture of orthorhombic and hexagonal structures was observed. According to the results of Rietveld refinement, the ratio between the 2 phases was 23% to 77%, with a dominant orthorhombic phase. The increased synthesis temperature prompted the formation of h-$YMnO_3$. Both XRD profiles of the samples prepared at 1000 °C and 1100 °C had more intense [004] diffraction peaks in comparison to the previously described compounds, suggesting a textured structure. The unit cell

parameters of these compounds are summarized in Table 1 and match well with the other samples prepared using a different precursors-to-chlorides ratio.

While metal halides are considered to be inert systems for molten salt synthesis, the use of nitrate salts, which have oxidizing properties, could potentially lead to several oxidative states for manganese ions in $YMnO_3$ or other samples. Another problem associated with molten salt synthesis is the possibility of doping of the final product with crucible material or salt medium cations, such as Na^+ or K^+ in our case. XPS analysis was performed in order to investigate the oxidation states of manganese ions, as well as to determine if any yttrium or manganese ions were potentially substituted with potassium or sodium ions. The results for $YMnO_3$ prepared at 1100 °C for 10 h with a nitrates-to-chlorides molar ratio of 1:10 are presented in Figure 6.

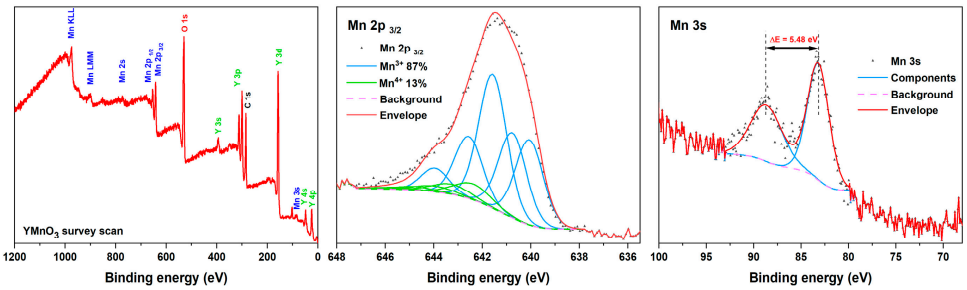

Figure 6. XPS spectra of $YMnO_3$ prepared at 1100 °C for 10 h with precursors-to-chlorides molar ratio of 1:10.

XPS can detect all elements except hydrogen and helium, probes the surface of the sample to a depth of 5–7 nanometers, and has detection limits ranging from 0.1 to 0.5 atomic percent depending on the element. In the XPS spectra of $YMnO_3$ (Figure 6), four different elements can be identified: Y, Mn, O, which constitutes the compound, and C, which gives additional signal unrelated with final sample. The additional high-resolution XPS spectra of Na 1s, K 2p, and K 2s were recorded and no subsidiary signals were detected, indicating no adventitious doping from the alkali salt medium. The analysis of Mn with different states is quite complicated due to the fact that the oxidation states are characterized by similar binding energies. For the determination of the manganese oxidation states, Mn 3s and Mn $2p_{3/2}$ spectra were recorded. The spin-orbit splitting ensuing in Mn $2p_{3/2}$ and Mn $2p_{1/2}$, as well as multiplet splitting, can be seen in the Mn +2, +3, and +4 spectra. The Mn^{2+} $2p_{3/2}$ spectrum revealed a distinctive satellite peak with a higher binding energy [39], which was not observed in our case, indicating the presence of the +2 oxidative state as highly improbable. Therefore, the $YMnO_3$ spectra was fitted with the Mn3+/4+ model, which revealed that the main oxidation state in this compound was +3 (87 to 13% in comparison with 4+ state). The small percentage of Mn^{4+} could be related to the formation of manganite on the surface. Moreover, the oxidation states could also be determined by comparing the energy differences in the Mn 2s spectra. The smallest difference could be observed for MnO_2 (around 4.7 eV) and largest for the MnO compound (ΔE~5.9 eV) [40]. In our sample, the measured ΔE value was around 5.5 eV, indicating that the majority of manganese ions were in the +3 oxidation state. This correlates well with the results of the structural and Rietveld analysis.

The morphology was analyzed for both samples prepared at 1000 and 1100 °C with the reaction time of 10 h and the ratio between nitrates and chlorides as 1:10; SEM micrographs are shown in Figure 7.

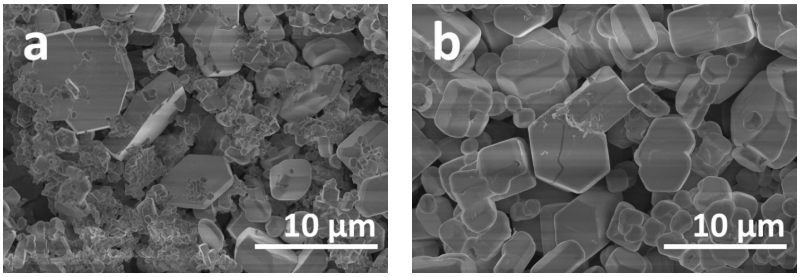

Figure 7. SEM micrographs of $YMnO_3$ prepared at 1000 °C (**a**) and 1100 °C (**b**) with the molar ratio between nitrates and chlorides as 1:10.

Notwithstanding synthesis temperature, both compounds demonstrated some particles with hexagonal shapes. In the case of the sample prepared at a lower reaction temperature (Figure 7a), larger hexagons were obtained in comparison with the specimen obtained at higher temperature (Figure 7b). The side length of hexagons in the first sample (Figure 7a) varied in the 1.5–4 µm range, while the other sample contained hexagons with 0.7–3 µm side lengths. Whereas the sample prepared at 1000 °C contained mostly hexagonal plates, the sample obtained at 1100 °C also consisted of hexagonal rods. Moreover, the sample (Figure 7a) prepared at 1000 °C also contained smaller particles in the nanometer range, while higher temperatures resulted in the formation of polyhedral particles with regular shapes only in the micrometer range. Not only the solid-state method could not be used to obtain hexagonally shaped particles, but other synthesis techniques, such as sol-gel [41] or sol-gel auto-combustion [42], did not produce hexagonal particles as well. Using these synthetic approaches, only spherical particles of nanoscale dimensions could be prepared. This indicates that our synthesis method could be applied to prepare particles with distinctive shapes.

It is known that smaller lanthanides can also form manganites ($LnMnO_3$) with hexagonal crystal structures. In order to investigate if our proposed synthetic approach was applicable for the preparation of other hexagonal manganites, additionally, we tried to synthesize Er, Tm, and Yb manganites using identical synthesis conditions (900 °C, the ratio between nitrates and chlorides as 1:2). The XRD patterns for these specimens are presented in Figure 8.

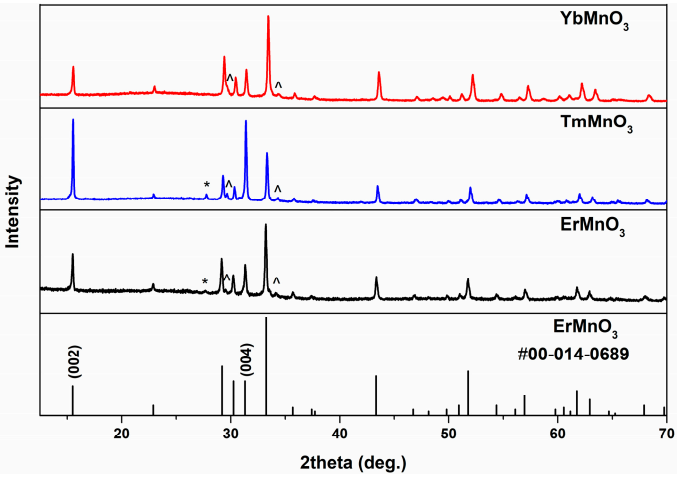

Figure 8. XRD patterns of $ErMnO_3$, $TmMnO_3$, and $YbMnO_3$. ^ represents respective lanthanide oxide phase, while * represents MnO_2.

In all cases, identical synthesis resulted in the formation of $REMnO_3$ with a hexagonal crystal structure; however, all samples additionally contained small amounts of lanthanide and manganese oxides as the neighboring phases. Additionally, $TmMnO_3$ demonstrated high-intensity (002) and (004) diffraction peaks, leading us to believe that this mixed oxide

has a specific texture, which similarly was the case for the $YMnO_3$ samples with higher amounts of chlorides. More intense (002) diffraction peaks can also be seen for $ErMnO_3$, as well as $YbMnO_3$.

SEM analysis was executed to determine if the hexagonally shaped particles formed when yttrium changed with the other lanthanides; the results are presented in Figure 9.

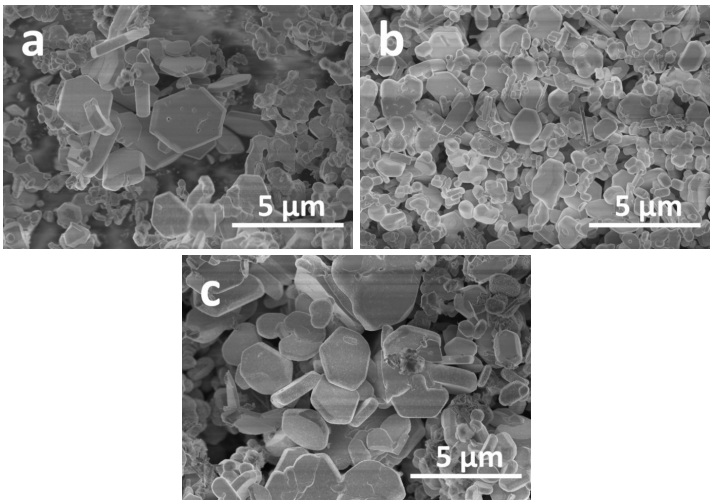

Figure 9. SEM micrographs of $ErMnO_3$ (**a**), $TmMnO_3$ (**b**), and $YbMnO_3$ (**c**) prepared at 900 °C with the molar ratio between nitrates and chlorides as 1:2.

Regardless of the chemical composition, all lanthanide manganites demonstrated the presence of hexagonally shaped plate-like particles. The size of these hexagons was slightly dependent on the lanthanide element. The side lengths of these hexagons for $ErMnO_3$ (Figure 9a) and $YbMnO_3$ (Figure 9c) were very similar and varied in the 0.5–2 µm range, while $TmMnO_3$ (Figure 9b) contained smaller hexagons—up to 1 µm in length. Additionally, all samples had smaller particles in the nanometer range without distinctive shapes.

3. Materials and Methods

3.1. Synthesis

For the preparation of $REMnO_3$ (RE = Y, Er, Tm, Yb), yttrium(III) oxide (Y_2O_3, 99.99%, Sigma-Aldrich, St. Louis, MO, USA), manganese(IV) oxide (MnO_2, Sigma-Aldrich, ≥99%), yttrium(III) nitrate hexahydrate ($Y(NO_3)_3{\cdot}6H_2O$, Sigma-Aldrich, 99.9%), erbium(III) nitrate hexahydrate ($Er(NO_3)_3{\cdot}6H_2O$, Sigma-Aldrich, 99.9%), thulium(III) nitrate pentahydrate ($Tm(NO_3)_3{\cdot}5H_2O$, Sigma-Aldrich, 99.9%), ytterbium(III) nitrate pentahydrate ($Yb(NO_3)_3{\cdot}5H_2O$, Sigma-Aldrich, 99.9%), and manganese(II) nitrate tetrahydrate ($Mn(NO_3)_2{\cdot}4H_2O$, 99.9%, Alfa Aesar, Haverhill, MA, USA) were used as the starting materials. Sodium chloride (NaCl, ≥99.5%, Carl Roth, Karlsruhe, Germany) and potassium chloride (KCl, Carl Roth, ≥99.5%) were used as the synthesis medium.

For the synthesis of $YMnO_3$, yttrium and manganese nitrates (the molar ratio between starting materials was 1:1) were taken and mixed with sodium and potassium chlorides in an agate mortar. The molar ratio between the sum of yttrium and manganese ions and chlorides was 1:2 or 1:10 (later, this ratio will be referred in the text as the nitrates to chlorides ratio), while the molar ratio between NaCl and KCl was 1:1. The mixture obtained after grinding was transferred to the corundum crucible and annealed at different temperatures (900 and 1100 °C) for different periods of time (1, 10, and 20 h). In all cases, the heating rate was set as 5 °C/min. The obtained products were taken out of the furnace and washed with a hot distilled water to dissolve the residual alkali metal chlorides. The obtained powders were filtered using a Büchner funnel and the presence of residual chloride ions was determined using a silver nitrate solution. This washing procedure was repeated 3 times for the complete separation of chlorides and the final product. All collected

powders were then dried in an oven at 80 °C for 1 h and ground in an agate mortar. For comparison, a similar synthesis procedure was conducted using yttrium and manganese oxides, with the main difference being that samples were annealed at 700 and 1100 °C for 10 h. The detailed procedure for the synthesis of $YMnO_3$ using oxides as the starting materials is reported elsewhere [27]. For the preparation of Er, Tm, and Yb manganites, an identical synthetic approach was applied, and specimens were prepared at 900 °C with the molar ratio between the nitrates and chlorides as 1:2.

3.2. Characterization

The thermal decomposition of nitrates in a mixture of chlorides was investigated by thermogravimetric and differential scanning calorimetric (TG/DTG/DSC) analysis using PerkinElmer STA 6000 Simultaneous Thermal Analyzer. About 5–10 mg of the sample was heated from 30 °C to 850 °C at 10 °C/min heating rate in a dry flowing air (20 mL/min). Powder X-ray diffraction (XRD) analysis was performed using Rigaku MiniFlex II diffractometer (Cu Kα, λ = 1.5419 Å) working in Bragg-Brentano (θ/2θ) geometry. The data were collected within the 10–70° 2θ range with a step of 0.02° and scanning speed of 1°/min. The obtained diffraction data were refined by the Rietveld method using the Fullprof suite. The Fourier transform infrared spectra (FTIR) were obtained in the range of 4000–400 cm^{-1} with a Bruker ALPHA-FTIR spectrometer with 4 cm^{-1} resolution. The morphology of the synthesized powders was analyzed by scanning electron microscopy (SEM) using Hitachi SU-70 microscope. The particle size was estimated from the SEM micrographs using ImageJ software (LOCI, Madison, WI, USA). The X-ray photoelectron spectroscopy (XPS) analyses were carried out with a Kratos Axis Supra spectrometer using a monochromatic Al-Kα source (25 mA, 15 kV). The instrument work function was calibrated to give a binding energy (BE) of 83.96 eV for the Au 4f7/2 line for metallic gold and the spectrometer dispersion was adjusted to give a BE of 932.62 eV for the Cu 2p3/2 line of metallic copper. The Kratos charge neutralizer system was used on all specimens. Survey (wide) scan analyses were carried out with an analysis area of 300 × 700 microns and a pass energy of 160 eV. High-resolution analyses were carried out with an analysis area of 300 × 700 microns and a pass energy of 20 eV. The spectra have been charge corrected to the main line of the carbon 1 s spectrum (adventitious carbon) set to 284.8 eV. The spectra were analyzed using CasaXPS software (version 2.3.23rev1.1R).

4. Conclusions

Hexagonal yttrium manganite ($YMnO_3$) was prepared with the simple, cheap, and non-sophisticated equipment required for the molten salt synthesis method. The in situ formation of oxides from the starting nitrates resulted in the formation of phase pure $YMnO_3$ in comparison to the synthesis, where oxides were used as the starting materials. By varying the synthesis temperature and the nitrates-to-chlorides ratio, a hexagonally shaped particles could be obtained. XPS analysis revealed that neither K^+ or Na^+ were doped into the $YMnO_3$ structure and the main manganese oxidation state was +3. By applying identical synthesis procedures, hexagonally shaped erbium, thulium, and ytterbium manganites can also be acquired. This synthetic approach where nitrates were used instead of oxides could potentially be applied for the preparation of similar oxide systems, as well as monocrystal growth.

Supplementary Materials: The following supporting information can be downloaded at: https://www.mdpi.com/article/10.3390/inorganics11050178/s1, Figure S1: XRD patterns of $YMnO_3$ prepared by using oxides as starting material; Figure S2: XRD patterns of $YMnO_3$ prepared at 900 °C with different reaction times.

Author Contributions: Conceptualization, D.K. and A.Z.; methodology, D.K.; formal analysis, D.K.; investigation, D.K., T.M. and A.Z.; resources, A.K.; data curation, D.K.; writing—original draft preparation, D.K. and T.M.; writing—review and editing, A.K.; supervision, A.Z. and A.K.; funding acquisition, A.K. and A.Z. All authors have read and agreed to the published version of the manuscript.

Funding: The work has been performed in frame of the TransFerr project. It has received funding from the European Union's Horizon 2020 research and innovation program under the Marie Skłodowska-Curie grant agreement No. 778070.

Informed Consent Statement: Not applicable.

Data Availability Statement: Not applicable.

Conflicts of Interest: The authors declare no conflict of interest.

References

1. Lilienblum, M.; Lottermoser, T.; Manz, S.; Selbach, S.M.; Cano, A.; Fiebig, M. Ferroelectricity in the Multiferroic Hexagonal Manganites. *Nat. Phys.* **2015**, *11*, 1070–1073. [CrossRef]
2. Das, H.; Wysocki, A.L.; Geng, Y.; Wu, W.; Fennie, C.J. Bulk Magnetoelectricity in the Hexagonal Manganites and Ferrites. *Nat. Commun.* **2014**, *5*, 2998. [CrossRef] [PubMed]
3. Lorenz, B. Hexagonal Manganites—(RMnO3): Class (I) Multiferroics with Strong Coupling of Magnetism and Ferroelectricity. *Int. Sch. Res. Not.* **2013**, *2013*, 497073. [CrossRef]
4. Li, M.; Tan, H.; Duan, W. Hexagonal Rare-Earth Manganites and Ferrites: A Review of Improper Ferroelectricity, Magnetoelectric Coupling, and Unusual Domain Walls. *Phys. Chem. Chem. Phys.* **2020**, *22*, 14415–14432. [CrossRef] [PubMed]
5. Manipatruni, S.; Nikonov, D.E.; Lin, C.-C.; Gosavi, T.A.; Liu, H.; Prasad, B.; Huang, Y.-L.; Bonturim, E.; Ramesh, R.; Young, I.A. Scalable Energy-Efficient Magnetoelectric Spin–Orbit Logic. *Nature* **2019**, *565*, 35–42. [CrossRef]
6. Ferson, N.D.; Uhl, A.M.; Andrew, J.S. Piezoelectric and Magnetoelectric Scaffolds for Tissue Regeneration and Biomedicine: A Review. *IEEE Trans. Ultrason. Ferroelectr. Freq. Control.* **2020**, *68*, 229–241. [CrossRef]
7. Arya, G.; Yogiraj, J.; Negi, N.S.; Shah, J.; Kotnala, R.K. Observation of Enhanced Multiferroic, Magnetoelectric and Photocatalytic Properties in Sm-Co Codoped BiFeO3 Nanoparticles. *J. Alloys Compd.* **2017**, *723*, 983–994. [CrossRef]
8. Mansour, S.F.; Imam, N.G.; Goda, S.; Abdo, M.A. Constructive Coupling between BiFeO3 and CoFe2O4; Promising Magnetic and Dielectric Properties. *J. Mater. Res. Technol.* **2020**, *9*, 1434–1446. [CrossRef]
9. Lee, K.; Hajra, S.; Sahu, M.; Kim, H.J. Colossal Dielectric Response, Multiferroic Properties, and Gas Sensing Characteristics of the Rare Earth Orthoferrite LaFeO3 Ceramics. *J. Alloys Compd.* **2021**, *882*, 160634. [CrossRef]
10. Huang, Z.J.; Cao, Y.; Sun, Y.Y.; Xue, Y.Y.; Chu, C.W. Coupling between the Ferroelectric and Antiferromagnetic Orders in $YMnO_3$. *Phys. Rev. B* **1997**, *56*, 2623. [CrossRef]
11. Zhang, Q.; Tan, G.; Gu, L.; Yao, Y.; Jin, C.; Wang, Y.; Duan, X.; Yu, R. Direct Observation of Multiferroic Vortex Domains in $YMnO_3$. *Sci. Rep.* **2013**, *3*, 2741. [CrossRef] [PubMed]
12. Griffin, S.M.; Lilienblum, M.; Delaney, K.T.; Kumagai, Y.; Fiebig, M.; Spaldin, N.A. Scaling Behavior and beyond Equilibrium in the Hexagonal Manganites. *Phys. Rev. X* **2012**, *2*, 041022. [CrossRef]
13. van Aken, B.B.; Palstra, T.T.M.; Filippetti, A.; Spaldin, N.A. The Origin of Ferroelectricity in Magnetoelectric $YMnO_3$. *Nat. Mater.* **2004**, *3*, 164–170. [CrossRef]
14. Wang, S.F.; Yang, H.; Xian, T.; Liu, X.Q. Size-Controlled Synthesis and Photocatalytic Properties of $YMnO_3$ Nanoparticles. *Catal. Commun.* **2011**, *12*, 625–628. [CrossRef]
15. Han, A.; Zhao, M.; Ye, M.; Liao, J.; Zhang, Z.; Li, N. Crystal Structure and Optical Properties of $YMnO_3$ Compound with High Near-Infrared Reflectance. *Sol. Energy* **2013**, *91*, 32–36. [CrossRef]
16. Addabbo, T.; Bertocci, F.; Fort, A.; Gregorkiewitz, M.; Mugnaini, M.; Spinicci, R.; Vignoli, V. Gas Sensing Properties of $YMnO_3$ Based Materials for the Detection of NOx and CO. *Sens. Actuators B Chem.* **2017**, *244*, 1054–1070. [CrossRef]
17. Tian, M.; Liu, X.; Gong, A.; Zhang, S.; Wang, G.; Han, P.; Li, Y.; Lou, X.; Hao, X. Efficient Ultraviolet–Visible-near Infrared Self-Powered Photodetector Based on Hexagonal $YMnO_3$-Based Ferroelectric Thin Film by Multiscale Polarity Structure Optimization. *Chem. Eng. J.* **2023**, *452*, 139040. [CrossRef]
18. Wadati, H.; Okamoto, J.; Garganourakis, M.; Scagnoli, V.; Staub, U.; Yamasaki, Y.; Nakao, H.; Murakami, Y.; Mochizuki, M.; Nakamura, M. Origin of the Large Polarization in Multiferroic $YMnO_3$ Thin Films Revealed by Soft-and Hard-X-Ray Diffraction. *Phys. Rev. Lett.* **2012**, *108*, 047203. [CrossRef]
19. Ahmad, T.; Lone, I.H.; Ubaidullah, M. Structural Characterization and Multiferroic Properties of Hexagonal Nano-Sized $YMnO_3$ Developed by a Low Temperature Precursor Route. *RSC Adv.* **2015**, *5*, 58065–58071. [CrossRef]
20. Turut, A.; Coşkun, M.; Coşkun, F.M.; Polat, O.; Durmuş, Z.; Çağlar, M.; Efeoğlu, H. The Current-Voltage Characteristics of the Ferroelectric p-$YMnO_3$ Thin Film/Bulk p-Si Heterojunction over a Broad Measurement Temperature Range. *J. Alloys Compd.* **2019**, *782*, 566–575. [CrossRef]
21. Ren, P.; Fan, H.; Wang, X. Bulk Conduction and Nonlinear Behaviour in Multiferroic $YMnO_3$. *Appl. Phys. Lett.* **2013**, *103*, 152905. [CrossRef]

22. DiSalvo, F.J. Solid-State Chemistry: A Rediscovered Chemical Frontier. *Science* **1990**, *247*, 649–655. [CrossRef] [PubMed]
23. Wang, M.; Wang, T.; Song, S.; Ravi, M.; Liu, R.; Ji, S. Enhanced Multiferroic Properties of $YMnO_3$ Ceramics Fabricated by Spark Plasma Sintering along with Low-Temperature Solid-State Reaction. *Materials* **2017**, *10*, 474. [CrossRef] [PubMed]
24. Gupta, S.K.; Mao, Y. Recent Developments on Molten Salt Synthesis of Inorganic Nanomaterials: A Review. *J. Phys. Chem. C* **2021**, *125*, 6508–6533. [CrossRef]
25. Gupta, S.K.; Mao, Y. A Review on Molten Salt Synthesis of Metal Oxide Nanomaterials: Status, Opportunity, and Challenge. *Prog. Mater. Sci.* **2021**, *117*, 100734. [CrossRef]
26. Ma, Y.; Chen, Y.; Wang, Z.; Liu, H.; Li, Y.; Wang, X.; Wei, H.; Cheng, G.J. Controllable Near-Infrared Reflectivity and Infrared Emissivity with Substitutional Iron-Doped Orthorhombic $YMnO_3$ Coatings. *Sol. Energy* **2020**, *206*, 778–786. [CrossRef]
27. Chen, Y.; Ma, Y.; Wang, Z.; Wang, X.; Liu, H.; Cheng, G.J. Molten Salt Synthesis of $YMnO_3$ Powder with High Near-Infrared Reflectivity. *Mater. Lett.* **2018**, *229*, 171–173. [CrossRef]
28. McBean, C.L.; Lewis, C.S.; Tiano, A.L.; Simonson, J.W.; Han, M.-G.; Gannon, W.J.; Yue, S.; Patete, J.M.; Corrao, A.A.; Santulli, A.C. A Generalizable Multigram Synthesis and Mechanistic Investigation of $YMnO_3$ Nanoplates. *Ind. Eng. Chem. Res.* **2017**, *56*, 5573–5585. [CrossRef]
29. Jian, G.; Xu, Y.; Lai, L.-C.; Wang, C.; Zachariah, M.R. Mn3O4 Hollow Spheres for Lithium-Ion Batteries with High Rate and Capacity. *J. Mater. Chem. A Mater.* **2014**, *2*, 4627–4632. [CrossRef]
30. Broström, M.; Enestam, S.; Backman, R.; Mäkelä, K. Condensation in the KCl–NaCl System. *Fuel Process. Technol.* **2013**, *105*, 142–148. [CrossRef]
31. Gizowska, M.; Piątek, M.; Perkowski, K.; Konopka, G.; Witosławska, I. Fabrication of Nanoyttria by Method of Solution Combustion Synthesis. *Nanomaterials* **2020**, *10*, 831. [CrossRef] [PubMed]
32. Saxena, P.; Mishra, A. Structural and Electrical Properties of $YMnO_3$ Manganites: Influence of Cr Ion Doping. *J. Solid State Chem.* **2021**, *301*, 122364. [CrossRef]
33. Karoblis, D.; Zarkov, A.; Garskaite, E.; Mazeika, K.; Baltrunas, D.; Niaura, G.; Beganskiene, A.; Kareiva, A. Study of Gadolinium Substitution Effects in Hexagonal Yttrium Manganite $YMnO_3$. *Sci. Rep.* **2021**, *11*, 2875. [CrossRef]
34. Rao, G.V.S.; Rao, C.N.R. Infrared and Electronic Spectra of Rare Earth Perovskites. Ortho- Chromites, -Manganites and -Ferrites. *Appl. Spectrosc.* **1970**, *24*, 436–444. [CrossRef]
35. Vishnuvardhan, T.K.; Kulkarni, V.R.; Basavaraja, C.; Raghavendra, S.C. Synthesis, Characterization and a.c. Conductivity of Polypyrrole/Y_2O_3 Composites. *Bull. Mater. Sci.* **2006**, *29*, 77–83. [CrossRef]
36. Cherian, E.; Rajan, A.; Baskar, G. Synthesis of Manganese Dioxide Nanoparticles Using Co-Precipitation Method and Its Antimicrobial Activity. *Int. J. Mod. Sci. Technol.* **2016**, *1*, 17–22.
37. Coşkun, M.; Polat, Ö.; Coşkun, F.M.; Durmuş, Z.; Çağlar, M.; Turut, A. Effect of Os Doping on Electrical Properties of $YMnO_3$ Multiferroic Perovskite-Oxide Compounds. *Mater. Sci. Semicond Process* **2019**, *91*, 281–289. [CrossRef]
38. Wan, F.; Li, L.; Bai, X.; Wang, Y.; Gao, L.; Li, J.; Cao, C. Structure and Dielectric Relaxation Behaviors of Co-Doped $YMnO_3$ Multiferroic Ceramics. *J. Mater. Sci. Mater. Electron.* **2022**, *33*, 17361–17371. [CrossRef]
39. Banerjee, D.; Nesbitt, H.W. XPS study of reductive dissolution of birnessite by oxalate: Rates and mechanistic aspects of dissolution and redox processes. *Geochim. Et Cosmochim. Acta* **1999**, *51*, 3025–3038. [CrossRef]
40. Ilton, E.S.; Post, J.E.; Heaney, P.J.; Ling, F.T.; Kerisit, S.N. XPS determination of Mn oxidation states in Mn (hydr)oxides. *Appl. Surf. Sci.* **2011**, *257*, 2717–2730. [CrossRef]
41. Joshi, Z.; Dhruv, D.; Rathod, K.N.; Boricha, H.; Gadani, K.; Pandya, D.D.; Joshi, A.D.; Solanki, P.S.; Shah, N.A. Low Field Magnetoelectric Studies on Sol–Gel Grown Nanostructured $YMnO_3$ Manganites. *Prog. Solid State Chem.* **2018**, *49*, 23–36. [CrossRef]
42. Chanu, L.P.; Phanjoubam, S. Study on the Structural and Electrical Properties of $YMnO_3$ Co-Substituted with Transition Metal Ions at Mn-Site and Their Conduction Mechanism. *J. Mater. Sci. Mater. Electron.* **2022**, *33*, 6107–6120. [CrossRef]